Thermal Breakthrough Calculations to Optimize Design of a Multiple-Stage Enhanced Geothermal System

Tianyu Li, Sogo Shiozawa, and Mark McClure

The University of Texas at Austin
Department of Petroleum and Geosystems Engineering, Austin, TX
mcclure@austin.utexas.edu

Keywords

EGS, multiple stages, thermal breakthrough, optimization, horizontal wells

ABSTRACT

We performed a simple optimization procedure and sensitivity analysis to examine designs for Enhanced Geothermal Systems (EGS) that involve horizontal wells and multiple fracturing stages. The sensitivity analysis included calculations of thermal breakthrough and the maximum flow rate that could be achieved through the system (considering pressure drop in the well and in the reservoir). Conventionally, EGS wells have been nearly vertical and stimulated in openhole sections in a single stage. We investigated a design involving two parallel horizontal wells. The first well would be drilled and completed with casing, and then stimulated sequentially in stages (using cased hole packers rated to high temperature). The second well would be drilled through the stimulated region created by the first and completed openhole. For different combinations of well spacing, fracture transmissivity, and number of stages, the optimal flow rate was determined to maximize present value (PV) of revenue (cost was not considered). The calculations showed that stimulating with multiple stages would radically improve economic performance, delaying thermal breakthrough and allowing a higher overall flow rate to be circulated through the system. At low well spacing and low number of stages, it is optimal to circulate fluid more slowly than the maximum possible rate, in order to delay thermal breakthrough. With greater well spacing and with more stages, thermal breakthrough will be relatively delayed, and it is optimal to circulate at the highest possible flow rate. It is optimal to use the lowest well spacing where NPV is maximized by circulating at the maximum possible rate. When it is optimal to circulate at the maximum possible rate, NPV is sensitive to reservoir transmissivity. When it is optimal to circulate at less than the maximum possible rate, NPV is unaffected by reservoir transmissivity. Optimizing to maximize aggregate heat extraction instead of NPV has only a limited effect on NPV. Most thermal drawdown calculations were performed assuming infinite stage spacing. Calculations assuming finite fracture spacing and a 1000 m lateral had only modestly lower NPV relative to the infinite fracture casing calculations.

1. Introduction

1.1 Premise

In Enhanced Geothermal Systems (EGS), hydraulic stimulation is used to increase the flow rate that can be achieved through a high temperature, low permeability formation. Fluid is circulated between injection and production wells. Cold water is injected and heats up as it flows through the formation toward the production well. The hot water or steam produced to the surface may be applied for direct use or for electricity generation.

Economic success for EGS requires that the time-discounted revenue from electricity or heat production is sufficient to offset expenses, plus provide an addition rate of return. An optimal EGS design would balance marginal cost and revenue to maximize time-discounted revenue minus expenses.

Project revenue is strongly affected by the temperature of produced fluid and the production rate, both of which are likely to change over time. Over the long term, the temperature of produced fluid will decline as the formation cools due to the loss of heat to the circulating fluid. It has been shown that an excessively high circulation rate may lead to poor heat sweep efficiency (Gringarten, 1975; Doe et al., 2014). On the other hand, the time value of money suggests that high circulation rate may be desirable because it will cause revenue to be earned as early as possible.

In this study, we used a simple conceptual model and relatively simple calculations to calculate optimal injection rates and well spacing (distance between injector and producer) for different wellbore configurations. Many simplifications are made, but the study provides a sensitivity analysis on the effect of different parameters and gives insight into the behavior of the optimization problem.

The primary objective of the study was to investigate the effect of multiple stage simulation on the economic performance of an EGS doublet. To date, most EGS projects have been performed

in nearly vertical wells, in a single stage, into openhole sections of wellbore. Two exceptions are the Schönebeck project, which used packers in several stimulation stages (Zimmermann et al., 2010), and the Newberry project, which used diverting agents to attempt an effectively multiple stage stimulation (Petty et al., 2013). We are interested in investigating the performance of an EGS doublet involving flow between parallel horizontal wells, as shown in Figure 1. In this design, a zonal isolation technology (such as packers) is used to pump sequentially into separate sections of one of the wellbores (referred to as multiple stage stimulation). The laterals are oriented so that the stimulated region at each stage forms roughly transverse to the horizontal lateral. Similar designs have been discussed by Gringarten et al. (1975), Green and Parker (1992), Nalla and Shook (2004), Jung (2013), and Shiozawa and McClure (2014).

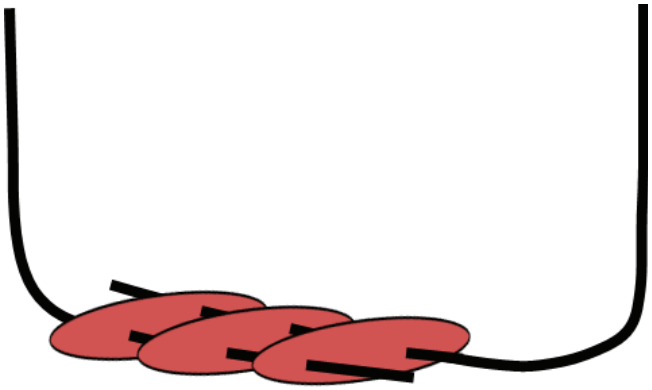

Figure 1. An EGS doublet of horizontal wells connected by vertical fracture stages (normal or strike-slip faulting regime). The wells are oriented toe to heel in order to encourage equal flow rates between stages.

In prior work, we discussed how using multiple stages would increase the maximum flow rate achievable through the system and showed how adding stages could dramatically increase flow rate (Shiozawa and McClure, 2014). The objective of this paper is to extend that work by investigating the effect of having multiple stages on thermal breakthrough. Thermal breakthrough is a complex function of many factors, including the overall flow rate through the system, the number of flowing fractures, the spacing between the laterals, and the spacing between the flowing fractures along the laterals. We performed a simple optimization to identify the ideal lateral spacing and flow rate, depending on the number of stages along the wells. We calculated the present value of the revenue derived from the system for different numbers of stages, assuming optimal well spacing and flow rate.

1.2 Conceptual Models for an EGS Reservoir

The classical EGS design has been based on the concept of shear stimulation, that an increase in fluid pressure induces slip on preexisting fractures, which experience a resulting increase in transmissivity. The hope has been that this process would create a large, closely spaced, well-connected network of natural fractures, which would access sufficient volume of rock to enable economically viable production.

Experience has revealed limitations to the conventional EGS design. Well logs have shown that flow tends to localize into a small number of widely space fractures at the wellbore (Richards et al., 1994; Ito and Kaieda, 2002; page 533 of Brown et al., 2012; Miyairi and Sorimachi, 1996; Wyborn et al., 2005; Baria et al., 2004; Dezayes et al., 2010). A careful investigation at the Soultz project suggested that only a handful of the critically stressed fractures at the wellbore actually appeared to become conductivity fluid pathways (Evans, 2005).

Numerical simulations based on continuum models of the reservoir, such as dual porosity models, tend to be overly optimistic and vastly underestimate the natural tendency for flow localization in fracture networks. Discrete fracture network simulations that couple fluid flow with the stresses induced by fracture deformation demonstrate how interaction of mechanical and hydraulic processes with the vagaries of flow in fracture networks creates localized deformation and sparsely populated fracture networks (McClure and Horne, 2010; McClure, 2013). Even if a large stimulated network is created, only a small minority of that network may actually be part of a strong hydraulic connection between an injection and production well (Section 2.4.3 from McClure, 2009). When flowing fractures are widely spaced, the heat sweep efficiency is unlikely to be optimal. Rapid thermal breakthrough has been observed at some EGS projects (Tenma et al., 2008).

A second problem has been establishing sufficient hydraulic connection between the injection and production wells. For example, this problem was documented at Fenton Hill (Brown et al., 2012), Rosemanowes (Parker, 1999), and the well GPK4 at Soultz (Genter et al., 2010).

The Soultz EGS project has achieved the highest circulating flow rate of any EGS project. But even at the Soultz project, the flow rate is not as high as needed. Furthermore, the Soultz project is in a location where there is already considerable natural permeability from preexisting large fault zones (Dezayes et al., 2010).

Unless proppant is used, we are unlikely to achieve greater flow rate on a per-fracture basis (and the efficacy and cost-effectiveness of proppant is uncertain). Therefore, the primary reason flow rates have been insufficient has been that not enough fractures have been stimulated and participated in a hydraulic connection between the injection and production wells. Any proposed strategy to improve economic performance for EGS must attempt to find a way to dramatically increase the number of flowing pathways that can be created in the reservoir.

Multiple stage hydraulic fracturing is an obvious candidate for improving the number of flowing pathways. When fluid is pumped into a lengthy wellbore section, fluid tends to flow into the first few fractures that form or that are stimulated at the wellbore. As a result, stimulation is not evenly distributed along the well. If the stimulation is performed with multiple stages, fractures are forced to form at each stage, creating a much more evenly spaced fracture network. In the oil and gas industry, the use of multiple hydraulic fracture stages has enabled a huge amount of new production from previously sub-economic shale formations (King, 2010).

An objection to the use of multiple stages in EGS has been that openhole packers have not been proven to work at high temperature. However, Shiozawa and McClure (2014) pointed out that in recent years, cased hole packers have become available that are rated to at least 200°C. EGS projects have nearly always been completed in openhole, both to save cost and to maximize contact with natural fractures (because the goal has been to stimulate

natural fractures). However, it is possible to perform stimulation out of perforated, cased wells. Bendall et al. (2014) reported on a well that was recently stimulated in granite at 3.68 km depth out of a perforated, cased well at 190°C.

Furthermore, we do not believe that shear stimulation is necessarily the best strategy for creating an effective EGS reservoir. An optimal EGS design would be highly repeatable, but shear stimulation is dependent on the local details of the natural fracture network. It may be advantageous in EGS to attempt conventional hydraulic fracturing, in which fluid is pumped out of the well with the intention of creating and propagating newly forming fractures. For a variety of reasons, investigators have predominantly claimed that the primary mechanism of stimulation in EGS is shear stimulation (summarized by McClure and Horne, 2013). McClure and Horne (2013) argued that, in fact, new fractures probably have formed and propagated at many EGS sites.

There are several operational decisions that could be made to increase the probability of new hydraulic fractures forming. If injection is performed into a perforated, cased hole, new fractures would be more likely to form than during pumping into openhole because the perforations would be unlikely to intersect natural fractures. Also, it has been observed in the oil and gas industry that the pumping of a more viscous fluid is more likely to create a "simple" fracture geometry, rather than a complex fracture network (Cipolla et al., 2008).

A "simple" fracture at each stage might appear to be undesirable because it would not create a large number of flowing fractures, which is required for a quality EGS reservoir. But the use of multiple fracturing stages would naturally create a large number of flowing features. Thus we propose to create a large number of "simple" fractures using multiple stages, rather than attempting to create a single massive fracture network from a single stage.

An important unknown is whether newly created hydraulic fractures would be capable of self-propping. The concept of shear stimulation relies on the mismatch of asperities to hold open natural fractures. Asperity mismatch may not occur on newly formed fractures. On the other hand, newly forming fractures may be sufficiently rough that they are able to self-prop, especially in hard rock such as granite (Jung, 1989).

Regardless of stimulation mechanism, either new fractures or shear stimulation of natural fractures, it is clear that having additional fracture stages would permit the formation of additional flow pathways by preventing injection fluid from diverting into a small number of features at the wellbore.

2. Methodology

To maximize the present value (PV) of an EGS doublet, we analyzed the effect of the four key elements in the fracture design: (1) flow rate, (2) the number of fracture stages, (3) the spacing between the two horizontal wells, and (4) fracture transmissivity. For each combination of parameters, an analytical expression was used to calculate the temperature of produced water over time. These values were converted into thermal production and electricity production, and finally, present value. For each combination of well spacing, fracture transmissivity, and number of stages, a variety of circulation rates were considered, up to the maximum possible rate, which was calculated by considering the pressure drop in the wells and in the reservoir. Different combinations of parameters were examined to find the optimal rate, spacing, number of stages and transmissivity. For comparison, we repeated the optimization maximizing the cumulative heat production instead of NPV.

2.1 Flow Rate Calculation

For each combination of parameters, the maximum flow rate possible through the system was calculated. The calculations included pressure gradient in the injection well, the reservoir, and the production well. Down to the target depth, the geometry of the injection and production wells was based on the deep wells GPK2 and GPK3 at the Soultz EGS project. However, unlike at Soultz, we assumed that at the target depth, the wells deviated to become horizontal. The wells were oriented toe-to-heel, as shown in Figure 1. For simplicity, the temperatures in the injector well, production well, and the reservoir were assumed to be constant (but different in each of the three).

The wellhead pressure of the injector, WHP_{inj}, and the wellhead pressure of the producer, WHP_{prod} were specified to be 4 MPa and 0.75 MPa, respectively (following the Soultz circulation test described by Tischner et al, 2006). Flow was also driven by the difference in density between the fluid in the injection well and the production well. Flow rate could have been increased by using a higher injection pressure, but practically, excessively high injection pressure may lead to excessive fluid loss. Flow rate could have been increased by pumping the production well, but this would involve additional cost and parasitic power loss. In practice, it would probably be economic to pump the production well, and it may be feasible to use a higher injection pressure than we assumed, but we chose these values in order to give conservative estimates.

For the calculation of pressure drop in the wells, it was assumed that all fluid entered or exited the wellbores at a single location, the middle of each of the two laterals (even though we were modeling wells with multiple stages). The system was modeled as four nodes connected in series: WHP_{inj}, BHP_{inj}, BHP_{prod}, and WHP_{prod}, where BHP_{inj} and BHP_{prod} are the bottomhole pressure of the injector and the producer wells, respectively. Wellbore pressure drop calculations were used to calculate ΔP_{inj}, equal to WHP_{inj} - BHP_{inj}, and ΔP_{prod}, equal to WHP_{prod} - BHP_{prod}. Darcy's law was used to calculate ΔP_{res}, equal to BHP_{inj} - BHP_{prod}. All fluid in the system was assumed to be single phase, liquid water.

For a given value of reservoir transmissivity, the flow rate through the system was calculated by numerically solving the following nonlinear equation, with flow rate, q, as the unknown:

$$WHP_{prod} = WHP_{inj} + \Delta P_{inj}(q) + \Delta P_{res}(q) + \Delta P_{prod}(q), \quad (1)$$

2.1.1 Pressure Change Calculation in the Injection Well and the Production Well

This section explains how $\Delta P_{inj}(q)$ and $\Delta P_{prod}(q)$ were calculated. The total pressure gradient (dp/dz) can be calculated as the sum of the frictional gradient $(dp/dz)_F$, the hydrostatic gradient $(dp/dz)_H$, and the accelerational gradient $(dp/dz)_A$ (Hasan and Kabir, 2002) and is given by:

$$(dp/dz) = (dp/dz)_F + (dp/dz)_H + (dp/dz)_A \quad (2)$$

The hydrostatic and the accelerational gradients are represented by:

$$(dp/dz)_H = -g\rho\sin\theta\,, \tag{3}$$

$$(dp/dz)_A = -(w/A)dv/dz = -\rho v dv/dz\,, \tag{4}$$

where ρ is the density of fluid, θ is the wellbore angle from horizontal line, w is the fluid mass of flow rate, A is cross-sectional area of casing, and v is its velocity.

The frictional pressure gradient is:

$$(dp/dz)_F = -fv^2\rho/2d\,, \tag{5}$$

where d is well or pipe diameter and f is friction factor, which depends on the turbulence of the fluid and also on the pipe roughness.

Chen (1979) proposed the following equation to calculate the Fanning friction factor:

$$f = \frac{1}{\left[2\log\left(\frac{\varepsilon/d}{3.7065} - \frac{5.0452}{\mathrm{Re}}\log\Lambda\right)\right]^2}\,, \tag{6}$$

where ε is pipe roughness, and A is the dimensionless parameter given by:

$$\Lambda = \frac{(\varepsilon/d)^{1.1098}}{2.8257} + \left(\frac{7.149}{\mathrm{Re}}\right)^{0.8981}\,. \tag{7}$$

Fluid properties were chosen for fresh water and are given in Table 1. The temperature in the injection well was assumed to be 60°C, and the temperature in the production well was assumed to be 180°C. The surface roughness of casing was assumed to be 150 microns, as estimated for the wellbore casing of GPK2 at Soultz by Mégel et al. (2005) based on measurements of the wellhead and bottomhole pressure during injection.

Table 1. Properties used in the flow rate calculations. The reservoir transmissivity shown is the "baseline" transmissivity.

Properties	Injector	Reservoir	Producer
Temperature (°C)	60	190	180
Fluid density (kg/m^3)	983.2	873.9	885
Fluid viscosity (cp)	0.466	0.142	0.151
Transmissivity (m^3)		3.07E-13	

Table 2 describes the geometry of the injection and production wells (based on the Soultz wells GPK2 and GPK3) including depth, casing diameter and inclination (Tischner et al., 2006). Table 2 contains the extended laterals on the horizontal wells (which were not present in GPK2 and GPK3). The wellbore lengths increased by 150 m for every stage that was added. The extended horizontal part of the injection well was assumed to be completed with casing and perforations (cased hole completion). The horizontal lateral of the production well was assumed to be openhole. The roughness of the formation in the openhole was assumed to be 2000 microns. Pressure drop in the perforations was not included in the calculation.

Table 2. Geometry and well head pressures of the injection well and production well.

Wellbore	MD (m)	Pipe Diameter (in)	Wellbore Angle From Horizontal (°)	WHP (MPa)
Injector	0-2373	9⅜	83.7	4
	2373-3449		70.9	
	3449-4282		70.9	
	4282-4550		90	
	4550-4610		75	
Injector possible extension (cased hole)	4610 – [4760-6110]	9⅜	0	
Producer	0-534	13⅝	90	0.75
	534-4084	7		
	4084-4638		79.2	
Producer possible extension (openhole)	4638 – [4788-6138]	8½	0	

Considering the flow geometry shown in Figure 1, each molecule of water will pass through the same length of wellbore lateral as it passes through the system (regardless of which stage it flowed through), and that length is equal to half of the total length of both the laterals. To account for this effect, every time a stage was added, the length of the horizontal lateral in both the injector and the producer was increased by one half the spacing between stages, 75 m.

2.1.2 Pressure Change Calculation in the Reservoir

This section explains how $\Delta P_{res}(q)$ was calculated. The pressure change through the reservoir was calculated from Darcy's law, assuming steady-state, linear flow through a fracture with height h (m) and transmissivity T (m^3):

$$\Delta P_{res} = \frac{q\mu D}{Th\rho} \tag{8}$$

where ΔP_{res} is BHP_{inj} - BHP_{prod} (MPa), q is flow rate of the reservoir (kg/s), μ is the viscosity of fluid (cp, or for unit consistency in Equation 8, MPa-s), and D is the distance between the injector and producer (m).

The Soultz project was used to make a baseline estimate for the transmissivity of an EGS reservoir. During the 2005 circulation test at Soultz, a 12 kg/s flow rate was sustained between GPK2 and GPK3. The openhole section of the wells was roughly 500 m and the well separation was roughly 600 m. Using those parameters, and using the reservoir and wellbore properties given in Table 1 and Table 2 (which were based on the Soultz circulation test), we estimated the overall reservoir transmissivity to be 3.07×10^{-13} m^3. We used this value as our baseline transmissivity for a single stage.

The exact nature and geometry of the fracture network at Soultz (or the network created in our hypothetical EGS system) is not important for the calculation. We are using a single number, reservoir transmissivity, to account for the aggregate flow capacity of the created fracture network, whether it was a single, planar

hydraulic fracture, a dense network of stimulated natural fracture, a large, thick, shear stimulated fault zone, or network of both new and preexisting fractures.

In our hypothetical EGS doublet, we assumed *h* to be 200 m. The wellbore spacing is a design parameter. When there were multiple stages, we assumed that flow was evenly distributed between each stage. Therefore, the flow rate per stage was q/S, where S is the number of stages. For application in Equation 8, the total system transmissivity equal to TS. Table 1 shows the fluid properties used in the calculations.

2.2 Heat Extraction from the Fractured Rock

We used the analytical solution developed by Gringarten et al. (1975) to calculate the fluid temperature at the producer as a function of time. This solution assumes a series of parallel planar fractures in the reservoir with height of h and spacing of L. The distance between the fractures is twice the half fracture spacing, X_e, and the total number of fractures (equal to the number of stages) is N. The water from the injection well flows through the fractures, gets heated up by the formation, and enters the production well. Figure 2 shows a schematic of the problem setup.

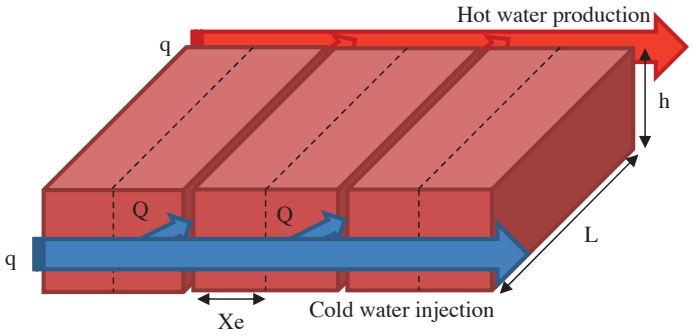

Figure 2. Illustration of the Gringarten et al. (1975) analytical solution.

In most of the calculations in this paper, we assumed that the half fracture spacing for our model was large enough that the spacing could be considered infinite. After manipulating the equation given by Gringarten et al. (1975) for single fracture, we got an idealized equation to calculate the water temperature at producer for multiple fractures with infinite fracture half spacing.

Defining T_{wo} for injecting temperature, T_{ro} for original formation temperature, K_r and K_w for thermal conductivity of rock and water respectively, c_r and c_w for the heat conductivity of rock and water, Q for the water injection rate per fracture per unit height, ρ_r and ρ_w for density of rock and water and t for production time, the following equation gives the water outlet temperature, T_w, assuming infinite fracture spacing:

$$T_w = T_{WO} + \left(T_{RO} - T_{WO}\right) * \mathrm{erf}\left(\frac{L * \sqrt{\left(K_R * c_R * \rho_R\right)/(t)}}{c_W * \rho_W * Q}\right),$$

where Q is calculated by using the total mass injection rate, q:

$$Q = \frac{q}{N * \rho_R * h}.$$

The values of the properties we put in the previous equations are shown in Table 3.

In some calculations (described in Section 3.6), we used the full solution of Gringarten et al. (1975), which calculates thermal drawdown for parallel fractures of finite spacing. The solution assumes a periodic boundary condition (infinite series of fractures). The solution requires a numerical inverse Laplace transform. To perform the calculation, we used a code that was written by Doe et al. (2014).

A very important input parameter was fracture height, set to 200 m. This parameter strongly affects the results, because it is proportional to the volume of fluid accessed during circulation. This is a difficult value to characterize, and 200 m was chosen as a fairly conservative value.

Table 3. Properties used in heat extraction calculations.

Properties	Symbols	Values	Units	Comments
Production time	t	946080000	s	Equivalent to 30 years
Fracture height	h	200	m	-
Formation temperature	T_{RO}	190	°C	-
Injecting temperature	T_{WO}	60	°C	-
Thermal conductivity of rock	K_R	3.01248	J/(m*s*°C)	For granite
Heat capacity of rock	c_R	1000	J/(kg*°C)	-
Heat capacity of water	c_W	4420	J/(kg*°C)	-
Rock density	ρ_R	2500	kg/m^3	-
Water density	ρ_W	873.9	kg/m^3	In formation
Number of stages	N	Varies	-	-
Well spacing	L	Varies	m	-
Injection rate	q	Varies	kg/s	-

2.3 Conversion to Electricity Production

The rate of thermal energy production from the EGS project was calculated with the following equation:

$$Q = qC_W\Delta T,$$

where the ΔT is changing with time, and q is mass flow rate (kg/s), C_w is the heat capacity of water (J/kg/°C), and ΔT is the temperature difference in the system (°C). When the produced fluid reached 150°C, it was assumed that no further electricity could be produced.

Cumulative electricity production was calculated by adding up the heat production for each specific time period during the production until the total production time td (years), and multiplying by efficiency, *eff*:

$$E(td) = \sum_{i=0}^{n} (Q * \Delta t_i * eff),$$

where n is the number of time periods. We assumed the energy conversion efficiency to be 12.63% (from Equation 7.1 from Tester, 2007).

2.4 Present Value (PV) Calculation

The NPV of the project was calculated by the following equation:

$$NPV(i,n) = \sum_{td=0}^{td=T} \frac{P * E(td)}{(1+i)^{td}},$$

where i is the discount rate, P is the price of electricity, td is the production time (years) and T is the total production time for the project (years). We assumed the price of electricity to be 5 cents per kWh and the discount rate to be 16%.

2.5 Present Value (PV) Optimization

We calculated the NPV for different combinations of parameters. The optimization algorithm was simple. Values were uniformly sampled throughout the solution space, and the combination of parameters that gave the highest NPV was selected. Because the truly optimal points lay between the sample points, this was an approximate optimization procedure. The distributions of parameters are given in Table 4.

Several separate optimization calculations were performed. For the first set of calculations, transmissivity was set to the baseline value of 3.07×10^{-13} m^3. We calculated the maximum possible flow rate for each combination of well spacing and stages. Then we found the optimal flow rate for each combination of parameters (which was sometimes equal to the maximum possible flow rate). Next, maximum NPV (using the optimal rate) versus the number of stages was calculated for each value of well spacing. Finally, the maximum NPV was calculated for each number of stages, using the optimal rate and spacing.

In the next set of analyses, the optimization procedure was performed using three different values of reservoir transmissivity. The analysis was performed for 200 and 800 meter well spacing.

In the third set of calculations, the optimization was performed with the objective of maximizing cumulative heat production instead of NPV. These calculations used the baseline value for transmissivity.

Finally, the optimization procedure was repeated using the baseline settings and finite fracture spacing, with a lateral length of 1000 m.

Table 4. The ranges of parameters in the optimization process.

Parameters	Minimum Value	Maximum Value	Total Number of Values	Distribution
Flow rate	qmax*log(-4)	qmax	40	log
Well spacing	100 m	800m	8	linear
Stages	1	30	30	linear
Transmissivity	1.02333E-13	9.21E-13	3	linear

3. Results

3.1 Maximum Flow Rate

Figure 3 shows the maximum possible flow rate for wells with specific number of stages and well spacing, assuming the transmissivity is $3.07*10^{-13}$ m^3.

3.2 Temperature and Cumulative Electricity Production Profile

Figure 4 shows the temperature and cumulative electricity production versus production time for a typical well with 30 stages and 400 m spacing.

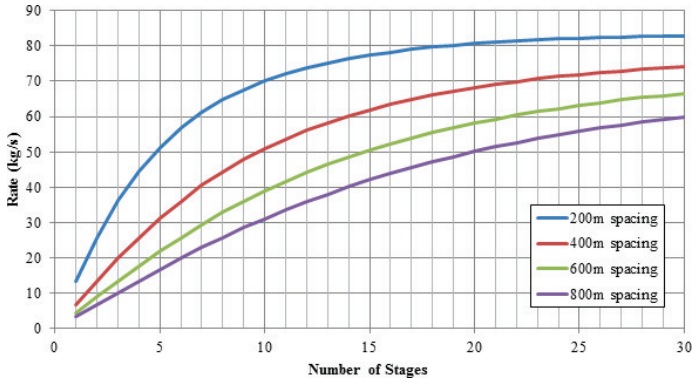

Figure 3. The maximum flow rate for wells with different spacing and stages.

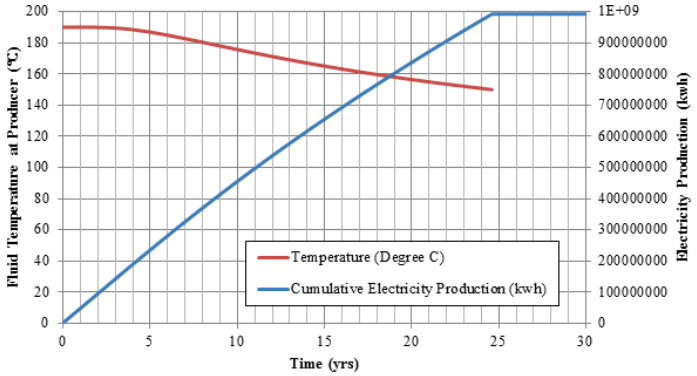

Figure 4. Typical temperature and cumulative production profile.

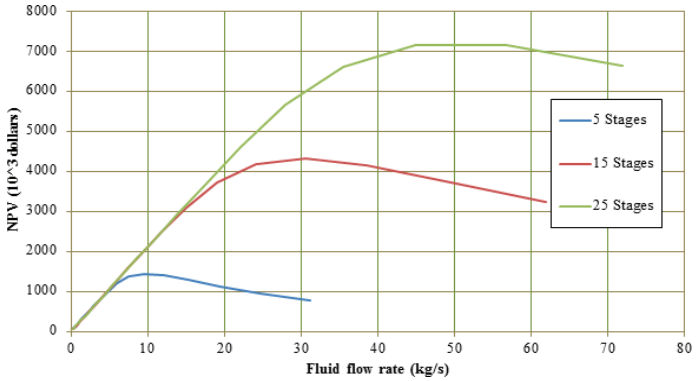

Figure 5. Net present value versus flow rate for 400 meter well spacing and 5, 15, and 25 stages.

3.3 Optimal NPV and Flow Rate for Different Well Spacing

As an example of the optimization performed by the code, Figure 5 shows NPV versus circulation rate for 400 meter spacing and 5, 15, and 25 stages. Figure 6 shows the fluid flow rate to achieve the optimal NPV for different values of wells spacing and number of stages. The optimal NPV for multiple well spacing settings versus the number of stages is given in Figure 7.

3.4 Optimal NPV for Different Transmissivity

Figure 8 and Figure 9 shows the optimal NPV under different transmissivity settings for wells with spacing of 200 m and 800 m respectively.

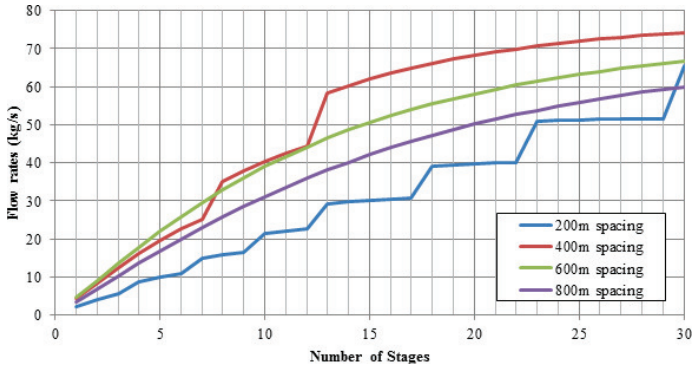

Figure 6. The rates to achieve optimal NPV for different spacing settings.

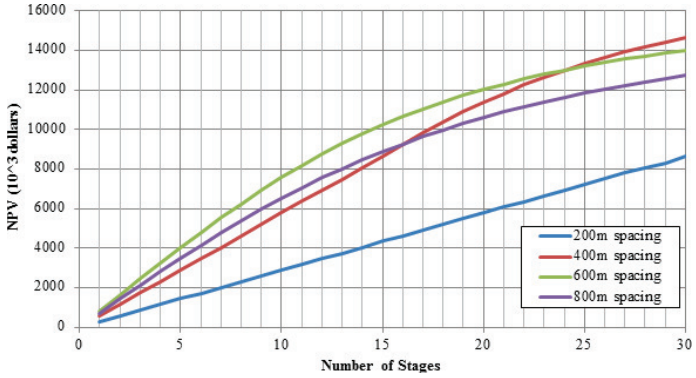

Figure 7. Optimal NPV for different spacing setting.

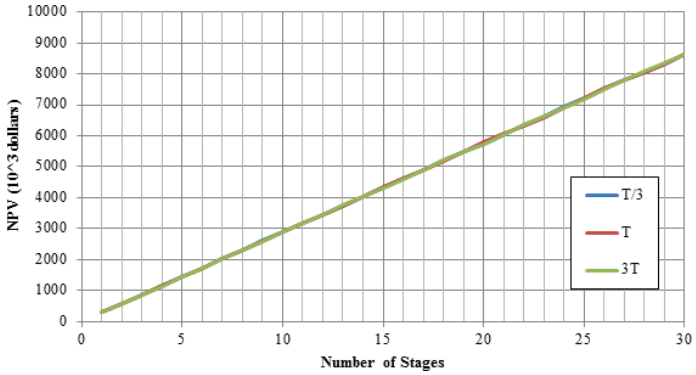

Figure 8. The optimal NPV for wells with 200 m spacing and different transmissivity.

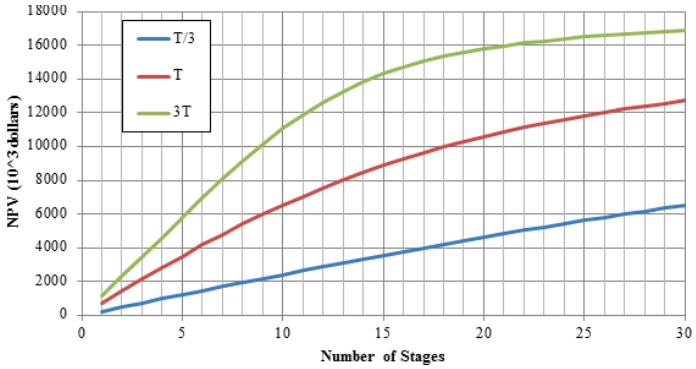

Figure 9. The optimal NPV for wells with 800 m spacing and different transmissivity.

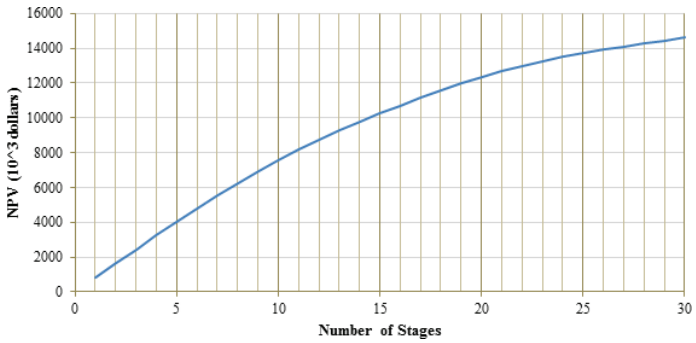

Figure 10. Maximum NPV with optimal combinations of flow rate and well spacing.

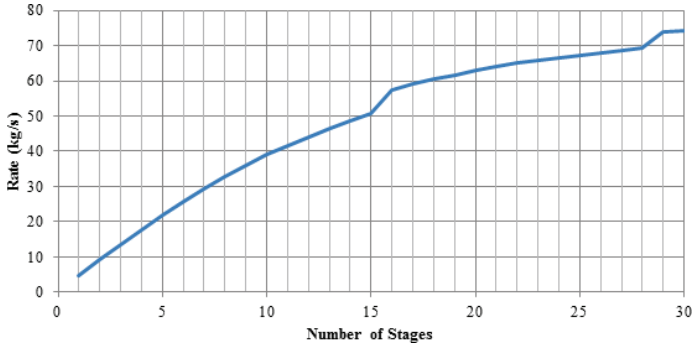

Figure 11. Optimal rates for each number of stages.

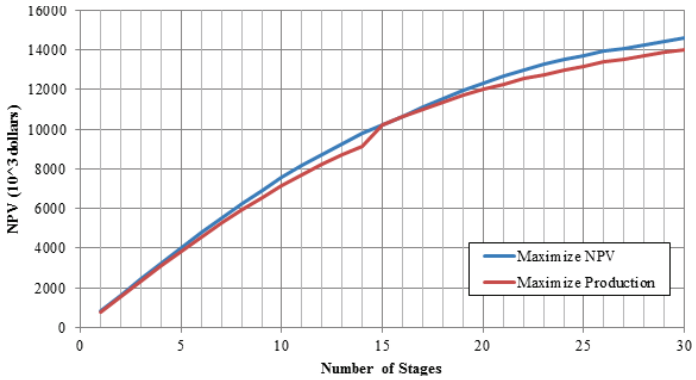

Figure 12. Comparison of the NPV between optimizing NPV and maximizing heat production.

3.5 Maximum NPV and Optimal Combination of Flow Rate and Well Spacing

Figure 10 shows the maximum NPV with the optimal combinations of flow rate and spacing for each number of stages. The optimal rate that generates the maximum NPV for the optimal combination of parameters is given in Figure 11.

3.6 Comparison Between Optimizing NPV and Maximizing Heat Production

Figure 12, Figure 13, Figure 14 show NPV, heat production, flow rate, and optimal well spacing depending on whether the procedure was designed to maximize NPV or total heat production.

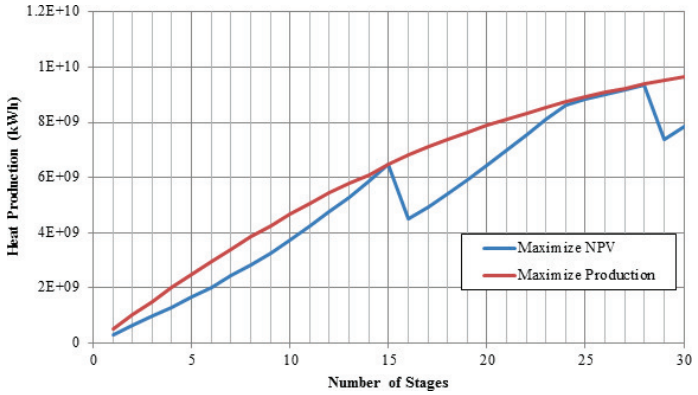

Figure 13. Comparison of the heat production between optimizing NPV and maximizing heat production.

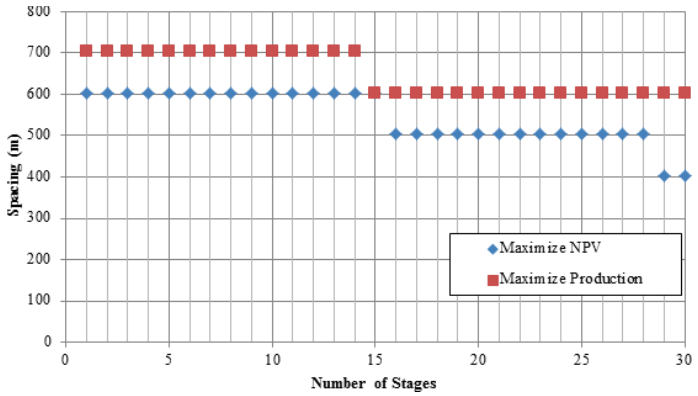

Figure 14. Comparison of the well spacing between optimizing NPV and maximizing heat production.

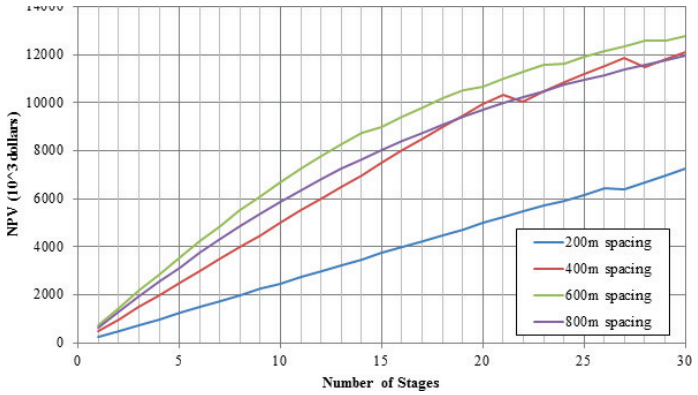

Figure 15. NPV versus number of stages with different values of fracture spacing using the finite fracture spacing Gringarten solution.

3.7 Effect on Finite Fracture Spacing

In the previous sections, spacing between the fracture stages was assumed infinite. This would only be an adequate assumption if the stages were adequately spaced. To test the effect of this assumption, we repeated the optimization using the full Gringarten et al. (1975) solution, which assumes finite fracture spacing. The total lateral length was assumed to be 1000 m. The spacing between stages was assumed to be the total lateral length, 1000 m, divided by the number of stages minus one.

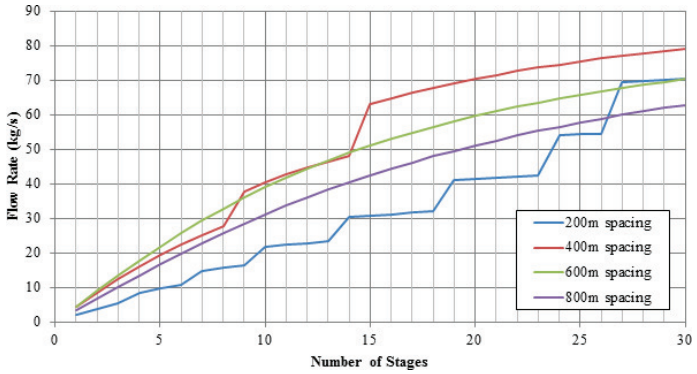

Figure 16. Optimal flow rate versus number of stages with different values of fracture spacing using the finite fracture spacing Gringarten solution.

4. Discussion

4.1 Maximum Flow Rate

Figure 3 shows the maximum flow rate through the system as a function of the number of stages and for different values of fracture spacing. The maximum rate is limited by pressure drop in the wellbore and in the reservoir. At low numbers of stages, the pressure drop is almost entirely in the reservoir. The pressure drop in the reservoir scales inversely with spacing, so greater rates are possible with lower spacing. The pressure drop in the reservoir scales linearly with the number of stages, and so as the number of stages grows larger, the proportion of pressure drop in the wellbores grows. As a result, flow rate through the systems grows roughly linearly with number of stages when there are fewer stages and greater well separation. As the overall pressure drop in the reservoir increases, the marginal effect of adding stages increases, as the pressure drop in the wellbore limits further increase in rate. This analysis was described in greater detail by Shiozawa and McClure (2014).

4.2 Thermal Drawdown

Figure 4 shows an example of produced temperature versus time for a particular combination of parameters. In this case, thermal drawdown begins after only a few years, but progresses slowly enough that the cutoff temperature of 150°C is not reached until nearly 24.5 years. For slower rates, the temperature decline is more gradual, but for higher rates, thermal decline can be rather abrupt.

4.3 Optimal Flow Rate

Figure 5 shows NPV as a function of circulation rate for 400 meter well spacing and 5, 15, and 25 stages. If circulation rate is too high, thermal breakthrough is too rapid and NPV is not maximized. If circulation rate is too low, thermal breakthrough is limited, but the productive capacity of the reservoir is not maximized. The curves do not extend beyond the maximum rate possible. In Figure 5, the optimal rate is always less than the maximum possible rate. But for some combinations of parameters, the optimal rate is equal to the maximum rate, and the curves monotonically increase.

Figure 6 shows the NPV-optimizing circulation rate as a function of the number of stages and for a variety of values for well spacing. Two distinct trends are apparent.

In cases with smaller number of stages and shorter well spacing, the optimal rate is limited by the potential for thermal breakthrough. Fluid is circulated more slowly than is possible through the system. For example, Figure 3 shows that for the one stage, 200 m spacing case, the maximum circulation rate is around 14 kg/s, but Figure 6 shows that the optimal rate is around to 2 kg/s. This is not an optimal design, because if the wells were spaced further apart, thermal breakthrough would be further delayed, and NPV would be increased. Increasing the spacing would lower the maximum circulation rate, but there would be no penalty because the optimal rate is lower than the maximum rate. Increasing the number of stages increases NPV (Figure 7) because it enables a higher total rate to be used without accelerating thermal breakthrough because it spreads flow over a greater number of fractures.

In cases with a greater number of stages and greater well spacing, it is optimal to circulate fluid at the maximum possible rate. In these cases, increasing the number of stages increases NPV (Figure 7) primarily because it increases the total flow rate through the system. In this case, increasing the well spacing further would not be advantageous because it would lower the total flow rate without having a sufficiently beneficial effect in delaying thermal drawdown. The optimal design occurs at the minimum well spacing where it is still optimal to circulate fluid at the maximum possible rate.

Figure 7 shows NPV (assuming circulation at the optimal rate) as a function of well spacing and number of stages. Except for the largest number of stages, the highest NPV is reached with the 600 meter well spacing. For 25 stages and larger, the 400 meter well spacing has higher NPV. With such a large number of stages, NPV is controlled by maximum flow rate, rather than thermal breakthrough, and lowering the spacing allows rate to be increased.

4.4 Effect of Reservoir Transmissivity

Figure 8 and Figure 9 show the NPV at optimal rate versus number of stages for three different values of reservoir transmissivity at well spacing of 200 m and 800 m, respectively. At low well spacing, the NPV is completely insensitive to reservoir transmissivity. This is because it is optimal to circulate fluid at much lower than the maximum rate. Unless the reservoir transmissivity was much lower, so that the maximum rate at 200 m spacing was less than the optimal rate, transmissivity would have no effect. At 800 m spacing, it is optimal to circulate at the maximum possible rate. As a result, the NPV is highly sensitive to reservoir transmissivity, because NPV is sensitive to the maximum possible rate.

This comparison somewhat exaggerates the effect of reservoir transmissivity because in practice, an optimal spacing could be selected based on reservoir transmissivity. A lower transmissivity reservoir would result in a closer optimal well spacing, partly countering the effect of lowering transmissivity.

At very high rates, wellbore pressure drop dominates, and it is not possible to increase flow rate much by increasing the number of stages. Therefore, for the highest transmissivity case, the 800 m spacing, and the largest number of stages, the marginal NPV for adding stages is limited.

4.5 Optimal Parameters

Figure 10 shows the optimal NPV as a function of the number of stages, assuming the optimal spacing and flow rate. In all cases, increasing the number of stages increases NPV. At lower circulation rate, increasing the number of stages results in a linear increase in NPV. Some diminishing return is seen, but even for 30 stages, there is considerable marginal NPV from adding stages. Increasing from one to thirty stages results in a roughly 15x increase in NPV.

Figure 11 shows the optimal flow rate for each number of stages, assuming the optimal well spacing. The optimal rate increases, as the addition of further stages increases the volume of rock accessed by the system, allowing heat to be extracted more rapidly with a similar thermal drawdown.

4.6 Optimizing NPV Versus Optimizing Cumulative Heat Extraction of 30 Years

Depending on project objectives, circulation rate may be chosen to optimize either NPV or cumulative heat extraction. Because we assumed a constant efficiency for converting heat to electricity, this was equivalent to maximizing total electricity production. An optimization based on NPV will favor higher rates because it is more valuable to produce electricity sooner. Figure 12 compares the NPV depending on if the rate and spacing are selected to maximize NPV or total electricity production. The optimization for total electricity production results in an NPV that is surprisingly close to the optimization for NPV. The nonsmoothness of the curve is caused by the error inherent to our inexact optimization algorithm. Figure 13 shows aggregate heat production for two cases: maximizing either NPV or heat production. In some cases, the heat production is nearly equal in the two cases, and in other cases they are fairly different. Figure 14 shows that the maximization of total production case tends to find a slightly greater well spacing to be optimal. The abrupt difference in total heat production between 15 and 16 stages (Figure 13) occurs because the optimization algorithm chooses to use a lower well spacing starting at 16 stages (Figure 14). The NPV between these two cases shows only a slight deviation (Figure 12), suggesting that in this case, decreasing well spacing results in only a slight increase in NPV, but a substantial drop in total heat production.

4.7 Finite Fracture Spacing

Figures 15 and 16 show the NPV versus number of stages and optimal rate versus number of stages for four values of well spacing, calculated using the Gringarten solution with finite fracture spacing (assuming a total lateral length of 1000 m). These figures can be compared to Figures 6 and 7, which were calculated with the Gringarten solution assuming infinite fracture spacing. The effect of the finite fracture spacing is greatest for the largest number of stages, when the spacing between each stage is smallest. The optimal fracture spacing is a bit greater. In this case, the 600 m spacing outperforms the 400 m spacing for 30 stages, unlike for the infinite spacing case, when the 400 m spacing has a higher NPV.

The optimal rate at 30 stages and 400, 600, or 800 m spacing turns out to be higher than for the infinite spacing case. In these cases, NPV is maximized by flowing at the maximum possible flow rate. In the cases where the infinite fracture spacing solution was used, the calculations of pressure loss in the wellbore assumed a spacing of 75 m. For 30 stages, this was an effective lateral length of 2175 m. The greater lateral length reduced the maximum possible flow rate relative to the finite spacing case.

The total optimal system NPV for 30 stages is only modestly lower for the finite fracture spacing case compared to the infinite fracture spacing calculation. This indicates that a lateral length of 1000 m accesses sufficient rock volume for economic production. Obviously, if the lateral length and stage spacing were too low, thermal drawdown would occur rapidly as all the heat stored in the rock volume was depleted. But further increases in lateral length beyond 1000 m may not result in much additional NPV.

A back of the envelope calculation can be performed to check this result. The volume of rock in a cube 1000x200x600 m is 1.2×10^8 m^3. Assuming a thermal drawdown of 40°C (from 190°C to 150°C), this volume contains 3.3×10^9 kWhr of heat. With a drawdown of 130°C (from 190°C to the injection temperature of 60°C), the heat content is 1.08×10^{10} kWhr. The latter value represents an upper bound on thermal recovery, achieved with perfect heat sweep efficiency and if the entire reservoir can be cooled to the injection fluid temperature before thermal breakthrough occurs. However, it neglects heat conduction from outside of the volume of rock (from the top, bottom, and sides). In the 30 stage, 600 m spacing case shown in Figures 15 and 16, the total heat production from the model was roughly 7.2×10^9 kWhr. This predicted recovery is theoretically possible, though clearly represents an aggressive assumption about heat sweep efficiency. On the other hand, the assumption of a "formation" height of 200 m may be conservative for a system with a spacing of up to 600 m.

Achieving high heat sweep efficiency would be significantly aided by the use of multiple stage fracturing, which would enable a large number of stimulated fractures to be formed. If a cased hole completion were used in one of the wells, packers could be used to isolate sections of the wellbore and pump diverting materials if some fracture pathways were excessively conductive. Flow through perforations from the cased hole would serve as a throttle that would prevent excessive rate from any particular stage. Because heat sweep is unlikely to be close to ideal, it would practically be desirable to overdesign the system, with a longer lateral and more stages than would be necessary, based on ideal sweep efficiency.

4.8 Practical Issues Affecting Well Spacing

Practically, there may be several disadvantages to attempting large well spacing, beyond 400-500 meters. First, as the size of the stimulated region increases, the volume of water required for injection will increase nonlinearly due to increased leakoff and increased height growth. The greater the distance between the injection and production wells, the more difficult it will become to establish a good connection between the wells. On the other hand, large stimulation designed for greater spacing may result in a greater effective fracture height than the 200 m assumed in our calculations.

5. Conclusions

Our most important result, consistent with the results of Shiozawa and McClure (2014), is that an EGS design with parallel horizontal wells and multiple stage fracturing delivers radically improved economic performance relative to conventional designs with a single stage and a vertical wellbore. Increasing the number of stages provides benefits because it increases the optimal circulation rate by allowing higher rates and delaying thermal breakthrough.

The optimal wellbore spacing occurs at the lowest possible spacing where NPV is maximized by flowing at the maximum possible flow rate through the system. Practically speaking, it may be advantageous to use a smaller spacing because this may reduce fracturing costs and increase the probability of establishing a good connection between the wellbores.

As long as the NPV is optimized by flowing at the maximum possible rate through the system, it is advantageous to increase fracture transmissivity (for example, by using proppant). This will occur unless the fracture transmissivity is already very high, or the well spacing is low.

Optimizing for maximum heat extraction rather than NPV had a surprisingly small effect on the results. It was found that, within the error of our approximate optimization scheme, the results were not too different. In some cases, it appeared that decreasing wellbore spacing may result in substantial loss of total heat extraction with minimal improvement of NPV.

For design of an actual multiple stage EGS doublet, a more sophisticated physical model and optimization scheme would be needed. In addition, optimal parameters would need to be calculated considering marginal costs. For example, adding stages would increase cost by requiring more casing, more cement, and a greater volume of water during stimulation. Increasing well spacing would increase water consumption needed per stage. In addition to marginal costs, a go/no go decision on a commercial EGS project would require considering of all costs associated with the project over the lifetime of the system. Because make-up wells could be drilled, EGS wells could be permitted to thermally decline at a timescale shorter than the life span of the power plant.

The calculations show that a lateral length of 1000 m is sufficient to access an adequate volume of rock. This length is comparable to many oil and gas wells drilled in unconventional resources.

This sensitivity analysis demonstrates that multiple stage fracturing designs radically improve EGS economic performance. Developing and testing technology that enables multiple stage fracturing and horizontal drilling for EGS needs to be a high priority for future development.

Acknowledgements

Thank you to the Cockrell School of Engineering at the University of Texas at Austin for supporting this research. Thank you very much to Thomas Doe for his thoughtful comments on this subject and also for sharing his code for implementing the Gringarten et al. (1975) finite fracture spacing calculation.

References

Baria, R., Michelet, S., Baumgärtner, J., Dyer, B., Gerard, A., Nicholls, J., Hettkamp, T., Teza, D., Soma, N., Asanuma, H., Garnish, J., and Megel, T. (2004), Microseismic monitoring of the world's largest potential HDR reservoir, paper presented at the Twenty-Ninth Workshop on Geothermal Reservoir Engineering, Stanford University, <https://pangea.stanford.edu/ERE/db/IGAstandard/record_detail.php?id=1702>.

Bendall, B., R. Hogarth, H. Holl, A. McMahon, A. Larking, and P. Reid (2014), Australian experiences in EGS permeability enhancement - a

review of 3 case studies, paper presented at the Thirty-Ninth Workshop on Geothermal Reservoir Engineering, Stanford University, <https://pangea.stanford.edu/ERE/db/GeoConf/papers/SGW/2014/Bendall.pdf>.

Brown, D. W., D. V. Duchane, G. Heiken, and V. T. Hriscu (2012), *Mining the Earth's Heat: Hot Dry Rock Geothermal Energy*, Springer-Verlag.

Chen, N. H. (1979), An explicit equation for friction factor in pipe, *Industrial & Engineering Chemistry Fundamentals*, *18*(3), 296-297.

Cipolla, C., N. Warpinski, M. Mayerhofer, E. Lolon, and M. Vincent (2008), The relationship between fracture complexity, reservoir properties, and fracture treatment design, SPE 115769, paper presented at the SPE Annual Technical Conference and Exhibition, Denver, Colorado, USA, doi:10.2118/115769-MS.

Dezayes, C., A. Genter, and B. Valley (2010), Structure of the low permeable naturally fractured geothermal reservoir at Soultz, *Comptes Rendus Geoscience*, *342*(7–8), 517-530, doi:10.1016/j.crte.2009.10.002.

Doe, T., R. McLaren, and W. Dershowitz (2014), Discrete fracture network simulations of Enhanced Geothermal Systems, paper presented at the Thirty-Ninth Workshop on Geothermal Reservoir Engineering, Stanford University.

Evans, K. F. (2005), Permeability creation and damage due to massive fluid injections into granite at 3.5 km at Soultz: 2. Critical stress and fracture strength, *Journal of Geophysical Research*, *110*(B4), doi:10.1029/2004JB003169.

Genter, A., K. Evans, N. Cuenot, D. Fritsch, and B. Sanjuan (2010), Contribution of the exploration of deep crystalline fractured reservoir of Soultz to the knowledge of enhanced geothermal systems (EGS), *Comptes Rendus Geoscience*, *342*(7-8), 502-516, doi:10.1016/j.crte.2010.01.006.

Green, A. S. P., and R. H. Parker (1992), A multi-cell design of a HDR reservoir, *Geothermal Resources Council Transactions*, *16*, 457-463.

Gringarten, A. C., P. A. Witherspoon, and Y. Ohnishi (1975), Theory of heat extraction from fractured Hot Dry Rock, *Journal of Geophysical Research*, *80*(8), 1120-1124, doi:10.1029/JB080i008p01120.

Hasan, A. R., and C. S. Kabir (2002), *Fluid flow and heat transfer in wellbores*, Society of Petroleum Engineers, Richardson, TX.

Ito, H., and H. Kaieda (2002), Review of 15 years experience of the Ogachi Hot Dry Rock Project with emphasis on geological features, paper presented at the 24th New Zealand Geothermal Workshop, <http://www.geothermal-energy.org/pdf/IGAstandard/NZGW/2002/Ito.pdf?>.

Jung, R. (1989), Hydraulic in situ investigations of an artificial fracture in the Falkenberg granite, *International Journal of Rock Mechanics and Mining Sciences & Geomechanics Abstracts*, *26*(3-4), 301-308, doi:10.1016/0148-9062(89)91978-5.

Jung, R. (2013), EGS - Goodbye or back to the future, in *Effective and Sustainable Hydraulic Fracturing*, edited by A. P. Bunger, J. McLennan and R. Jeffrey, pp. 95-121, InTech, doi:10.5772/45724

King, G. (2010), Thirty years of gas shale fracturing: what have we learned?, SPE 133456, paper presented at the SPE Annual Technical Conference and Exhibition, Florence, Italy, doi:10.2118/133456-MS.

McClure, M. W. (2013), Understanding, diagnosing, and modeling the causes of fracture network complexity in unconventional reservoirs, *The Leading Edge*, *32*(12), 1494-1500, doi:10.1190/tle32121494.1

McClure, M. W., and R. N. Horne (2010), Discrete fracture modeling of hydraulic stimulation in Enhanced Geothermal Systems, paper presented at the Thirty-Fifth Workshop on Geothermal Reservoir Engineering, Stanford University, <https://pangea.stanford.edu/ERE/db/IGAstandard/record_detail.php?id=5675>.

McClure, M. W., and R. N. Horne (2013), Conditions required for shear stimulation in EGS, paper presented at the European Geothermal Conference, Pisa, Italy, <https://pangea.stanford.edu/researchgroups/scits/sites/default/files/EGC2013_PS2-03.pdf>.

Mégel, T., T. Kohl, A. Gérard, L. Rybach, and R. Hopkirk (2005), Downhole pressures derived from wellhead measurements during hydraulic experiments, paper presented at the World Geothermal Congress, Antalya, Turkey, <http://www.geothermal-energy.org/pdf/IGAstandard/WGC/2005/1636.pdf>.

Miyairi, M., and M. Sorimachi (1996), Characterization of effective fractures by production logging at Hijiori HDR test site, paper presented at the Second Well Logging Symposium of Japan, Chiba, Japan, <www.japexrc.com/ptfd.files/PTF2ndSymp.pdf>.

Nalla, G., and M. Shook (2004), Engineered Geothermal Systems using advanced well technology, Geothermal Resources Council Transactions, 28, 117-123. Parker, R. (1999), The Rosemanowes HDR project 1983–1991, *Geothermics*, *28*(4–5), 603-615, doi:10.1016/S0375-6505(99)00031-0.

Petty, S., Y. Nordin, W. Glassley, T. T. Cladouhos, and M. Swyer (2013), Improving geothermal project economics with multi-zone stimulation: results from the Newberry Volcano EGS Demonstration, paper presented at the Thirty-Eighth Workshop on Geothermal Reservoir Engineering, Stanford, CA, <http://www.geothermal-energy.org/pdf/IGAstandard/SGW/2013/Petty.pdf>.

Richards, H. G., R. H. Parker, A. S. P. Green, R. H. Jones, J. D. M. Nicholls, D. A. C. Nicol, M. M. Randall, S. Richards, R. C. Stewart, and J. Willis-Richards (1994), The performance and characteristics of the experimental Hot Dry Rock geothermal reservoir at Rosemanowes, Cornwall (1985–1988), *Geothermics*, *23*(2), 73-109, doi:10.1016/0375-6505(94)90032-9.

Shiozawa, S., and M. McClure (2014), EGS designs with horizontal wells, multiple stages, and proppant, paper presented at the Thirty-Ninth Workshop on Geothermal Reservoir Engineering, Stanford, CA, <http://www.geothermal-energy.org/pdf/IGAstandard/SGW/2014/Shiozawa.pdf>.

Tenma, N., T. Yamaguchi, and G. Zyvoloski (2008), The Hijiori Hot Dry Rock test site, Japan evaluation and optimization of heat extraction from a two-layered reservoir, *Geothermics*, *37*, 19-52, doi:10.1016/j.geothermics.2007.11.002.

Tischner, T., M. Pfender, and D. Teza (2006), Hot Dry Rock projekt Soultz: erste phase der erstellung einer wissenschaftlichen pilotanlage: Final project report. Bundesanstalt für Geowissenschaften und Rohstoffe (BGR), <http://www.bgr.bund.de/DE/Themen/Energie/Downloads/soultz_abschlussbericht.pdf?__blob=publicationFile&v=2>.

Wyborn, D., L. de Graaf, S. Davidson, and S. Hann (2005), Development of Australia's first Hot Fractured Rock (HFR) underground heat exchanger, Cooper Basin, South Australia, paper presented at the World Geothermal Congress, Antalya, Turkey, <https://pangea.stanford.edu/ERE/db/IGAstandard/record_detail.php?id=1473>.

Zimmermann, G., A. Reinicke, G. Blöcher, I. Moeck, G. Kwiatek, W. Brandt, S. Regenspurg, T. Schulte, A. Saadat, and E. Huenges (2010), Multiple fracture stimulation treatments to develop an Enhanced Geothermal System (EGS) - conceptual design and experimental results, paper presented at the Word Geothermal Congress, Bali, Indonesia, <http://www.geothermal-energy.org/pdf/IGAstandard/WGC/2010/3106.pdf>.